SELF-PROPELLED MOTION OF FILM BOILING DROPLETS

ON RATCHET-LIKE SURFACES

by

LAURA MELLING

A THESIS

Presented to the Department of Physics
and the Honors College of the University of Oregon
in partial fulfillment of the requirements
for the degree of
Bachelor of Arts

June 2003

APPROVED:_____
Dr. Heiner Linke

An Abstract of the Thesis of

Laura Dian Melling   for the degree of   Bachelor of Arts

in the Department of Physics   to be taken   June 2003

Title: SELF-PROPELLED MOTION OF FILM BOILING DROPLETS ON

       RATCHET-LIKE SURFACES

Approved:_____

           Dr. Heiner Linke

We have observed a novel phenomenon by which asymmetrically structured surfaces can be used to direct the motion of film boiling droplets without applying an external force to the system. Droplets placed on such a surface move in a preferred direction, and under common conditions accelerate in that direction. In this thesis, we present a phenomenological description of the observed behavior, and develop a mathematical model for the motion of droplets on ratchet and non-ratchet surfaces. Using this model, we show that asymmetry is a requisite of the observed behavior. We also show that surface and droplet properties influence the resulting acceleration.

To Ruth, Ted, and Gavin. Thanks for making me laugh.

TABLE OF CONTENTS

LIST OF FIGURES, TABLES, AND EQUATIONS

TABLES:

EQUATIONS:

$$v(t) = \left[v(0) - \frac{F_{constant}}{\beta} \right] e^{-\frac{\beta}{m}t} + \frac{F_{constant}}{\beta}$$

$$= \left[v(0) - \frac{a_{constant}}{\beta/m} \right] e^{-\frac{\beta}{m}t} + \frac{a_{constant}}{\beta/m}$$

$$a_{other} = a_{drag} + a_{ratchet} = -\frac{\beta}{m}v + a_{ratchet}$$

PREFACE

We have observed a novel phenomenon by which asymmetrically structured surfaces can be used to direct the motion of film boiling droplets without applying an external force to the system. Droplets placed on such a surface, which will be referred to as a ratchet, move in a preferred direction, and under common conditions accelerate in that direction. For small inclines (~ 2 degrees), this acceleration has been observed to move the droplet uphill, overcoming the countering gravitational acceleration. The purpose of this research is to formulate a model for the system that is able to explain the observed behavior of the droplets.

INTRODUCTION

Ratchets are transport mechanisms relying on forces generated by local asymmetry and non-equilibrium conditions. Often described as "force-free" motion, the large-scale motion produced by a ratchet is actually due to local forces that have an average of zero over space and time. Many such ratchet devices have been studied [1-10]. Some ratchet mechanisms, including the classic *Feynman's ratchet* explained below, use asymmetry in shape. Others rely on local asymmetry in applied force, provided that the average force is zero. Disequilibria in a ratchet can be due to a thermal gradient, but in many cases it is due to a periodic alteration of the system over time, such as switching on and off a local force.
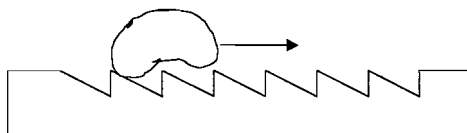
Figure 1: A schematic diagram of our ratchet with a nitrogen droplet.
The droplet moves to the right.

A liquid nitrogen droplet (temperature, T $\approx$ 77 K = -196°C) and a room

temperature surface (T $\approx$ 300 K = 27°C) are far from *thermal equilibrium*. Based on the

knowledge that ratchet systems combine disequilibria with local asymmetry to produce

motion, we predicted that the droplets might move on a surface with broken symmetry.

Upon testing this idea, it was determined that such an effect did exist. Liquid nitrogen

droplets (radius, r $\sim$ 1 mm; volume, V $\sim$ 10^{-6} liters) placed on a periodic asymmetric

surface move in a preferred direction (see Figure 1). The purpose of our current research

is to determine the specific physical processes responsible for the observed motion of the

droplets.

A number of researchers are interested in various methods for transporting

droplets and pumping liquids. Such methods have applications in a wide variety of

microfluidic technologies, including "lab-on-a-chip" devices for microchemical analysis

of compounds [10-12], DNA transport and separation techniques [3,6,10,12,13], and

propulsion of micromachines [5], as well in more conventional devices such as heat

exchangers [13]. A multitude of schemes have arisen which employ macroscopic

chemical or thermal gradients to produce droplet motion [4,11,13-23]. The various

methods involving chemical gradients typically utilize a contact angle gradient resulting

from a hydrophobicity gradient in order to move droplets [4,13,15-20,22]. Temperature

gradients have been used to move droplets by means of the associated Marangoni flow

[14,16,23,24]. Some systems using the principles of "force-free" motion to pump liquids have also been studied [2,3,5,6,9,10]. An overview of these effects is given below.

BACKGROUND

BASIC THERMODYNAMIC PRINCIPLES

Equilibrium is, by definition, the state at which all evolution has ceased. That is, when a system is in equilibrium, any process that occurs will happen equally often in one direction as the opposite direction, leaving the state of the system unchanged. An important consequence of equilibrium is that no useful work can be extracted [1]. When a system is not in equilibrium, it must by definition have a preferred direction it tends to evolve (i.e., toward the equilibrium state). Any system left for a sufficient period of time will reach equilibrium, unless energy is expended in order to keep the system away from equilibrium.

Thermal equilibrium is the condition when two objects have the same temperature. Temperature is, in simple terms, an indicator of the thermal energy, or heat, of an object. When objects are out of thermal equilibrium, thermal energy will flow toward the cool object until they reach equilibrium (i.e., until they are the same temperature). As an example of this process, consider a hot cup of coffee left sitting on the kitchen table. The kitchen and the coffee are out of thermal equilibrium because the temperature of the coffee is greater than the ambient temperature of the kitchen. What thermodynamics and experience tells us is that the coffee will cool off, giving up thermal energy to the surrounding room. When the coffee and the kitchen are out of thermal equilibrium, heat will tend to flow in a preferred direction (i.e., from the hot object to the

cooler one). On the other hand, when objects are in thermal equilibrium, heat is not transferred in any preferred direction, and the temperature of each object will remain fixed. Thus once our cup of coffee has cooled to the temperature of the kitchen, it will neither heat back up nor cool past room temperature.

Because of this spontaneous evolution toward the equilibrium state (and corresponding transfer of energy), it is possible to extract useful work from a non-equilibrium system [1]. Thus, although droplets can appear to be "self-propelled" and even climb uphill with no external force, there is no reason to worry that these phenomena violate conservation of energy. In the case of the behavior we present, the energy required to produce motion is spontaneously transferred to the liquid nitrogen droplet due to the temperature gradient between the droplet (T $\approx$ 77 K) and the ambient environment (T $\approx$ 300 K).

RATCHETS

In order to see how local asymmetry and disequilibria can be used to produce motion, consider the system in Figure 2. This theoretical device, known as *Feynman's ratchet*, has been studied extensively [25,26]. One section consists of a wheel with asymmetric teeth and a pawl held against the teeth by a spring, while the other section is a group of paddles. An axle connects the two sections. The size of the device is very small, such that interactions of individual air molecules with the spring and the paddles are significant. The spring is damped so that when displaced from its equilibrium length it will return to equilibrium, rather than continually oscillating. When the spring is holding the pawl in place, motion in one direction ("forward") is easier due to the asymmetry.
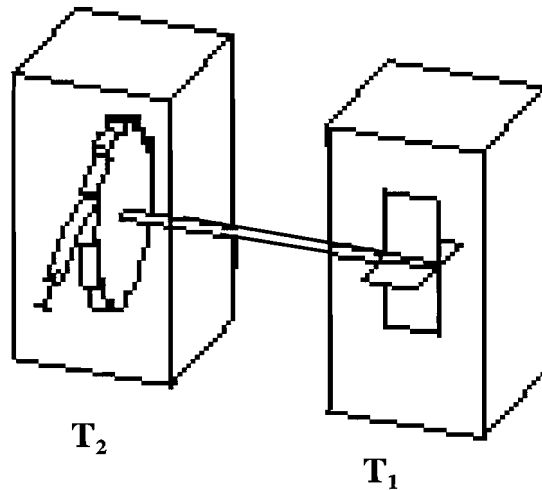
Figure 2: The Feynman Ratchet. A wheel with asymmetric teeth and a pawl held in place by a spring form a ratchet. The ratchet is connected to a paddle wheel.

In order to lift the pawl enough for the wheel to rotate, we require an amount of energy, which we call ε. We assume rotation of the device requires negligible energy. When an air molecule hits either part of the device, it imparts a portion of its energy to it. If the molecule hits a paddle, the whole apparatus will attempt to rotate. The asymmetric teeth of the wheel will restrict motion resulting from collisions with the paddles to the forward direction. If the paddles gain an energy of at least ε, in the proper direction, the ratchet will rotate forward. However, if the pawl gains an energy ε, it can lift enough for the wheel to move in either direction before it falls back into place. When the pawl is randomly lifted the device could rotate freely due to any collision with the wheel or the paddles. The spring and pawl will force the wheel to rotate until the pawl rests in a minimum of the tooth shape. Due to the asymmetry of the ratchet teeth, the distance needed to rotate back one "tooth" is a much shorter distance than that required to rotate forward one. In this case, when the pawl lifts, the wheel will move backward much more

often than forward. We thus get forward motion from collisions with the paddles alone, and backward motion from collisions with the pawl. Since we always have collisions with both ends, we need to determine which motion dominates to know what direction the ratchet will turn.

The temperature of the air surrounding the device is related to the frequency of the collisions, and the energy they impart to the device. In *thermal equilibrium*, the temperatures are the same and the air molecules will collide with each end at equal rates, and with equivalent energies. Therefore "forward" motion caused by molecules colliding with the paddles is cancelled out by "backward" motion from collisions with the pawl, and no directed motion is produced. Now assume that by some means we are able to control the temperature of the gas surrounding the paddles (T_1) and the ratchet (T_2) separately. If $T_1 > T_2$, then the increased collisions with the paddles will drive the ratchet forward. If $T_2 > T_1$, then increased collisions with the pawl result in a net backward motion. Thus when we are out of thermal equilibrium, it is possible to use asymmetry to extract useful work [1,26].

<center>**SELF-PROPELLED DROPLETS**</center>

Chemical Gradients / Wettability

Many droplet transport mechanisms utilize gradients in the chemical properties of a surface to create a gradient in wettability [13,16,18-20,27]. *Wettability*, usually quantified through the *equilibrium contact angle*, is a measure of how energetically favorable it is for a liquid to spread across a surface. An energetically favorable state is one with low energy, which can be thought of as low "cost". A *contact angle* is the angle

between the solid surface and the tangent line to the droplet at the point of contact with

the solid (see Figure 3). We note that droplets placed on a smooth homogenous surface

will take a symmetric, spherical cap shape [10].
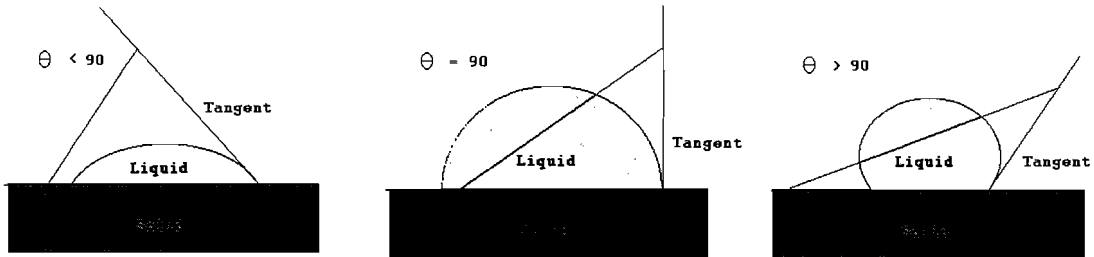
Figure 3: Three examples of equilibrium contact angles (increasing from right to left) for different solid-liquid-gas systems. The equilibrium contact angle for each system depends on the interfacial energies.

Through a simple energy consideration, we can determine the equilibrium contact

angle of a droplet on a surface. A well-established principle of physics states that for a

system at constant pressure, minimization of a quantity called the *Gibbs free energy* is

equivalent to reaching thermodynamic equilibrium. Gibbs free energy is essentially the

amount of energy I would need spend to create a system. When a droplet sits on a solid

surface three interfaces must be considered: solid-liquid, solid-vapor, and liquid-vapor.

Each interface has a corresponding Gibbs free energy per unit surface area, γ_{SL}, γ_{SV}, and

γ_{LV} respectively, which depends on the two substances forming the interface. The liquid-

vapor surface free energy, γ_{LV}, is more commonly known as *surface tension*, and all three

energies represent the energy required to form a unit area of each interface [28].

The total interfacial Gibbs free energy, G^s, is given by the sum of the surface

areas multiplied by their respective areal energies, γ. By changing the solid-liquid

contact area by an amount ΔA, while keeping the volume of the droplet fixed, the contact

angle must change by a small amount $\Delta\theta$. This small change in shape generates a change in the surface Gibbs free energy [28]:

$$\Delta G^S = \Delta A(\gamma_{SL} - \gamma_{SV}) + \Delta A \gamma_{LV} \cos(\theta - \Delta\theta)$$

where $\Delta A \cos(\theta - \Delta\theta)$ is the change in the liquid-vapor surface area. Minimization of the total Gibbs free energy of the surfaces leads to an expression, known as Young's equation [28], for the equilibrium contact angle, θ_e,

$$\cos\theta_e = \frac{\gamma_{SV} - \gamma_{SL}}{\gamma_{LV}}.$$

A low equilibrium contact angle indicates that the droplet wants to spread on the surface, while a high θ_e means the droplet will remain more spherical (see Figure 3).

By creating a gradient in the wettability, and thus in θ_e, it is possible to use the resulting energy gradient to drive droplets into motion. For example, Chaudhury and Whitesides [18] used a gradient in surface energy to induce motion of water droplets toward a region of low equilibrium contact angle. A simplified picture of how this works is shown in Figure 4.
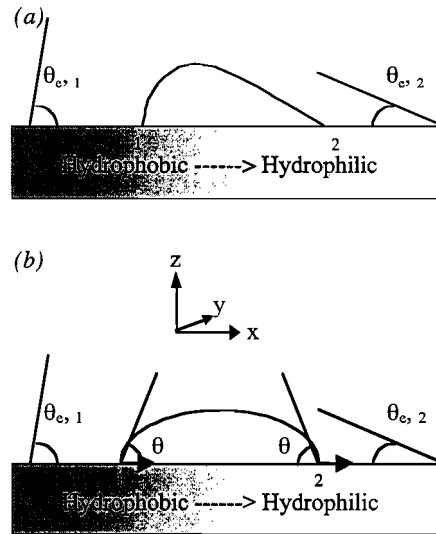
Figure 4: A droplet on a surface with a hydrophobicity gradient. (a) The droplet shape if both contact angles were satisfied and (b) the actual shape achieved.

Chaudhury and Whitesides used a surface with a *hydrophobicity* gradient. A gradient in the hydrophobicity of a surface is a gradient in the solid-liquid and solid-vapor surface free energies due to a varying chemical composition of the solid surface. This gradient in free energies leads to a changing equilibrium contact angle along the x-direction – the hydrophobic region has high θ_e (as in Figure 3 (c)), while the hydrophilic region has low θ_e (as in Figure 3 (a)). We consider the case of a smoothly varying θ_e. If the droplet were to satisfy both equilibrium contact angles, the droplet would become asymmetric, as in Figure 4 (a). However, the droplet will tend to assume a symmetric spherical-cap shape in order to maintain a balance of the hydrostatic pressure within the droplet. A combination of surface tension and pressure effects will determine the actual shape. For simplicity, we assume the pressure effects dominate, leading to a symmetric droplet with a contact angle θ satisfying $\theta_{e,2} < \theta < \theta_{e,1}$ (see Figure 4 (b)). In general, the

two angles will be slightly different, but the following argument still holds. At the hydrophobic edge of the droplet the actual contact angle is less than the equilibrium contact angle ($\theta < \theta_{e,1}$), causing the liquid to want to contract inwards (to the right in the diagram) in order to reach equilibrium. At the hydrophilic side of the droplet the actual angle is larger than the equilibrium angle ($\theta > \theta_{e,2}$), causing the droplet to expand radially outwards (also to the right). Thus the droplet will experience a net movement to the right (toward the hydrophilic region) in an attempt to reach equilibrium.

More rigorously, the free energy gradient can be treated as a potential energy gradient. A spatial gradient in potential energy leads to a force toward the region of lower potential energy. Like a ball rolling down a ramp, the water droplet moves toward the "downhill" (hydrophilic) region due to the decreased potential energy. If a section of the droplet with thickness Δy is moved a small distance dx to the right (see Figure 5), we replace an area $\Delta y \bullet dx$ of solid-liquid interface at point 1, with an equal area at point 2 (and vice-versa for the solid-vapor interface).

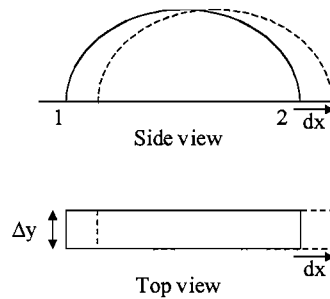Figure 5: Diagram of cross-sectional slice of a droplet (thickness Δy) displaced by a distance dx.

The resulting change in Gibbs free energy is:

$$dG^S = [(\gamma_{SL} - \gamma_{SV})_2 - (\gamma_{SL} - \gamma_{SV})_1]\Delta y \cdot dx$$

where the subscripts 1 and 2 refer to the free energies at the corresponding endpoints shown in Figure 5. This potential energy gradient leads to a force, known as Young's Force [18], on the strip in the x direction, given by:

$$F_{Young}(x) = -\frac{dG^S}{dx}$$
$$= [(\gamma_{SV} - \gamma_{SL})_2 - (\gamma_{SV} - \gamma_{SL})_1]\Delta y$$
$$= \gamma_{LV}[\cos\theta_{e,2} - \cos\theta_{e,1}]\Delta y$$

which is non-zero due to the gradient in θ_e, and is in the positive x-direction since $\theta_{e,1} > \theta_{e,2}$ and the cosine function is decreasing on the range of possible angles (0 –180 degrees).

Experimentally, Chaudhury and Whitesides [18] were able to use such a force resulting from a hydrophobicity gradient to send water droplets (~2mm in length) uphill an angle of 15° traveling at ~ 1 mm/s. This principle can also be utilized on originally homogeneous surfaces, by placing a reactive chemical into the droplets [19,20]. For example, by putting a *surfactant* (a chemical which reacts to make the surface hydrophobic) into the droplet, the surface underneath the droplet will become increasingly hydrophobic with time. As a droplet moves, the front edge will be least hydrophobic, and the rear most hydrophobic, since the surfactant at the front has had much less time to react with the surface. Thus, the droplet will be continually out of equilibrium, with the advancing edge having a lower equilibrium contact angle than the receding edge of the droplet. Accordingly, the droplet will move away from its trail via the Young's force, continually trying to reach equilibrium (see Figure 6).
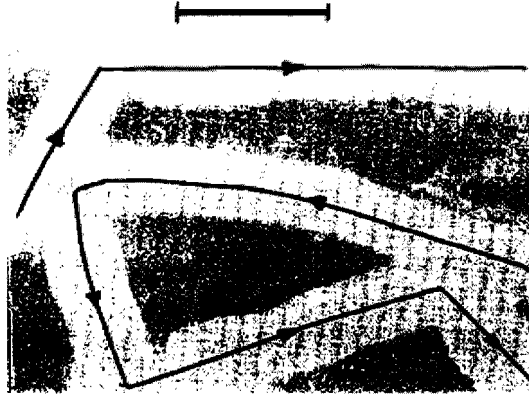
Figure 6: Image of the path followed by a surfactant-laden droplet. From reference [19].

Thermal Gradients / Marangoni Effect

More closely related to our experiments are the systems using temperature gradients to produce droplet or liquid motion. Temperature gradients used to move liquids are actually a subset of a more general phenomenon called the *Marangoni effect*. The term *Marangoni effect* describes liquid flow caused by a gradient in surface tension [28,29]. (Such flows are also referred to as capillary motion [30]). *Surface tension* is the common term for the liquid-vapor interfacial Gibbs free energy, but it is also used to refer to a liquid-liquid free energy, γ_{L1-L2}, in the context of an interface between two liquids. For simplicity, in the following paragraphs we adopt the notation of γ to refer to surface tension.

If a gradient in surface tension is present, the liquid near the interface will tend to flow toward the region of higher surface tension [23,30]. The motion, called Marangoni flow, is due to a surface shear stress (force tangential to the surface per unit area), τ, exerted by the surface on the surrounding liquid [31]. The shear stress is given by:

$$\tau = \frac{d\gamma}{dx},$$

where x is a coordinate measured along the curved interface. The shear stress is simply the rate of change of the surface tension along the interface. Several factors, including temperature, pressure, and surfactant concentration can influence the surface tension of a liquid. By creating a gradient in any of these quantities, we would expect the resulting surface tension gradient to produce a Marangoni flow near the surface, and possibly a movement of the bulk liquid.

A familiar example of the Marangoni effect is the "tears" or "legs" of wine creeping up the sides of a wine glass [28]. The surface tension of wine depends on its alcohol concentration – decreased alcohol concentration increases surface tension. Alcohol is a volatile liquid that will evaporate at room temperature, while the rest of the wine (mostly water) will evaporate at a much lower rate. When a liquid is in a container (such as a wine glass), the region near the edges forms a thin curved region called a meniscus. The uppermost portions of the meniscus will have low alcohol concentrations, due to evaporations. This gradient in alcohol concentration leads to a surface tension gradient. Consequently, the wine near the surface will flow upward, toward the region of high surface tension. The process will continue until the size of the droplet is such that the downward force due to gravity is larger than the upward force created by the surface tension gradient. At this point the droplets fall back into the wine.

A number of other phenomena due to the Marangoni effect have been studied, many of which employ thermal gradients [14,16,17,23,24,29]. Bulk motion resulting from a temperature-induced Marangoni flow is also known as *thermocapillary flow* [29]. In the case of thermocapillary flow, the tangential stress can be written as:

$$\tau = \frac{d\gamma}{dx}$$

$$= \frac{d\gamma}{dT}\frac{dT}{dx}$$

which is the product of the rate at which the surface tension varies with temperature and the rate at which the temperature varies tangential to the surface.

As an example of thermocapillary driven motion, we consider the historically influential paper by Young et al. [23]. Their apparatus consisted of a container of oil with a vertical temperature gradient. In the absence of a temperature gradient, air bubbles submerged in a liquid will rise due to the buoyant force (a force due to the difference in density). However, air bubbles injected into the oil were observed to migrate toward the (warmer) bottom.

In general, bubbles or droplets inside a bulk liquid are attracted to warm regions. We can understand this motion in terms of energy minimization. For most liquids, surface tension decreases with increasing temperature. Thus, the surface energy of the interface is comparatively low in regions where the temperature of the bulk liquid is high. If the bubble moves toward the warm region, each segment of the interface is at a higher temperature and therefore the total surface energy will decrease. This energy gradient leads to a force in the direction of the warm region.

More specifically, when a vertical temperature gradient (cold at the top and warm at the bottom) is present in the bulk oil there will be, in particular, a temperature gradient across the bubble. The surface tension will be higher in regions of low temperature, in this case in the higher portions of the liquid. The surface tension gradient that arises will cause the liquid at the interface to flow upwards. This upward flow causes the gas bubble

to react, migrating downward toward the warm region [23]. For large enough temperature gradients, this force overcomes the buoyant force that drives the droplet upward.

Marangoni flow can also be used to move droplets on solid surfaces, rather than within another liquid. For example, Daniel *et al.* used a surface with both a thermal gradient and a hydrophobicity gradient to produce accelerated motion of water droplets (r~ 0.2 mm) at speeds up to 1.5 m/s [13].

Local Asymmetry/ Ratchet Motion

Another subset of droplet transport mechanisms related to the effect we present are those employing the principles of "force-free" motion. "Lab-on-a-chip" and other miniaturized devices require the pumping of small amounts of liquids ($\sim 10^{-9}$ liters) through narrow channels at high speeds. This can be difficult using conventional pumping techniques, which typically employ macroscopic gradients (such as chemical or pressure gradients) to move liquids from one point to another. The efficiency of these methods decreases drastically with miniaturization. For a pressure gradient, as the channel decreases in radius, the velocities obtained decrease as the radius to the fourth power [2]. On the other hand, devices utilizing local gradients and asymmetry to produce bulk flow can actually increase in efficiency with miniaturization, requiring only very small gradients to produce significant velocities [3,5].

For example, Sandre *et al.* [10] use sawtooth shaped surfaces and an oscillating voltage to move water droplets. Their system consists of a water droplet spanning between two charged capacitor plates, with the remaining volume between the plates filled with oil. Each capacitor plate is coated with an insulating film that is imprinted with a sawtooth profile. The droplets cover several sawtooth periods.

For a droplet sitting on a ridged surface, the contact point will be "pinned" to the ridge tops [10]. The pinning is due to the fact that the contact angle is not strictly defined at the ridges, and the droplet can assume any angle within the sector defined by the equilibrium contact angle with the right and left-hand slopes. This sector is the shaded region in Figure 7. The dark black line indicates the actual angle at which the droplet intersects the ridge. On both sides of the droplet the sector will be the same size, but due to the asymmetry the left-hand sector will not be a symmetric reflection of the right-hand sector.

When a droplet is placed on the insulating layer coating the (positive or negative) capacitor plate, the drop will want to spread out in order to reduce its electrostatic energy [10]. The decrease in electrostatic energy that occurs when the droplet spreads offsets the increase in surface energy that results from the increased surface area. This process, known as electrowetting, can be thought of as a reduction in the effective surface tension of the droplet. The reduced surface tension causes a decrease in the equilibrium contact angle θ_e. Thus, a droplet will spread when an electric field is applied.
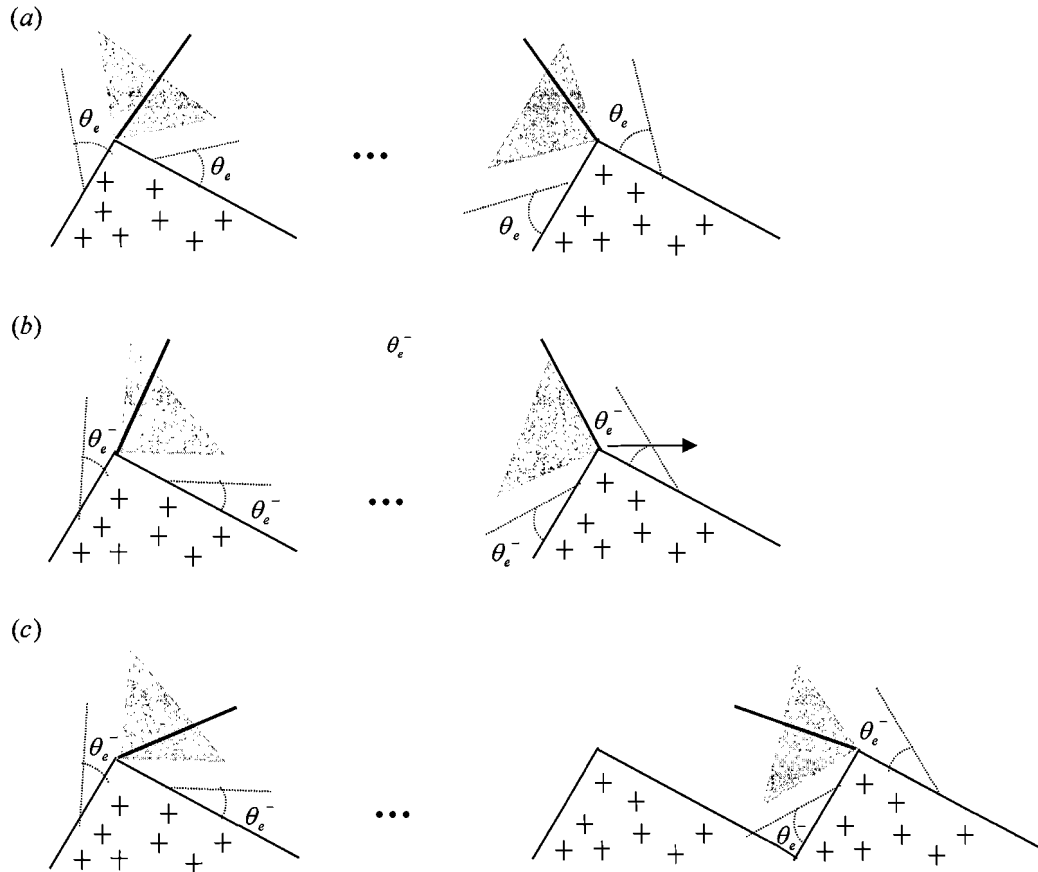
Figure 7: Schematic diagram of droplet motion on a sawtooth shaped surface induced by varying the magnitude of an electric field. The dark line is the actual contact angle of the droplet. The shaded regions indicate the angular sector within which the actual contact angle may lie. (a) The original configuration with no electric field. (b) When an electric field is turned on, the equilibrium contact angle will decrease. At a given equilibrium contact angle, θ_e^-, the droplet will jump one ridge to the right. (c) The configuration after the jump has taken place.

In Figure 7, this decrease in θ_e corresponds to a rotation of the angular sectors – the left-hand sector will rotate clockwise, while the right-hand sector will rotate counter-clockwise. If the electric field is increased, the equilibrium contact angle will steadily decrease. The droplet will remain "happy" until the right-hand sector has rotated enough so that the actual contact angle of the droplet "leaves" the allowed sector. At this point, the actual contact angle at the right-hand side of the droplet is larger than the new (smaller) equilibrium contact angle, which we shall call θ_e^-. The angle θ_e^- is chosen

small enough that the contact angle on the right side remains inside that sector, which is possible due to the asymmetry. In order to decrease its contact angle the right-hand side of the droplet will expand, moving to the right by one period. When this happens, the droplet will spread out to a lower actual contact angle, since the left-hand side contact point is still pinned (see Figure 7 (c)).

Now that the droplet is at this lower actual contact angle (shown by the thick black line), we can turn down the electric field, and thereby increase the equilibrium contact angle. Again, the configuration of the droplet will remain unchanged until the contact angle at either edge is no longer inside the appropriate sector. However, this time the left-hand side contact angle will be the first to leave its sector, at a certain angle θ_e^+. In this case, the actual contact angle will be smaller than θ_e^+, so the droplet will contract. This causes the left-hand edge of the droplet to move one ridge to the right. Therefore, turning an electric field on and off one time produces a motion of two jumps to the right.

When applying an alternating electric field to the capacitor plates, the amplitude of the field will constantly cycle between zero and some maximum value. Using such a field, Sandre et al. were able to repeat the process described above in a cyclic manner. Applying a field with a 50 Hz oscillation, 10 microliter water droplets were observed to move at speeds of 0.15 mm/s [10].

A number of other ratchet mechanisms for droplet transport use similar techniques. Gorre et al. [8] and Buguin et al. [6] have induced the motion of droplets in asymmetric capillaries by applying an oscillatory force with a time average of zero. Others have used asymmetric electrode arrays to produced flow of bulk liquids [3,5].

OUR SYSTEM/FILM BOILING

Our system is comprised of a liquid nitrogen droplet on a ratchet with periodic asymmetric grooves (see Figure 1). The ratchet is at room temperature (~300K) and the liquid nitrogen is at its boiling point (77K). Due to the temperature gradient, heat is transferred to the droplet, which undergoes evaporation (boiling). Because the temperature of the ratchet is significantly higher than the boiling point of liquid nitrogen, the evaporation would be very rapid if the droplet touched the surface. However, as the droplet nears the surface, the large amount of vapor released causes a build-up of excess pressure beneath the droplet. This pressure results in a force that lifts the droplet, moving it away from the surface and leaving a vapor layer between the drop and the surface. The vapor layer insulates the drop, dramatically slowing the heat transfer rate, and thus the evaporation rate. This in turn leads to a decrease in the pressure beneath the droplet, causing the droplet to fall slightly. For a droplet on a smooth surface, the droplet settles into an equilibrium height above the surface (~50 micrometers for nitrogen, see [32]), where the pressure due to evaporation is just enough to support the weight of the droplet, but not lift it.

This type of boiling, where the liquid does not touch the surface, is called *film boiling* [33,34]. The temperature at which film boiling initiates is known as the *Leidenfrost temperature* [33]. The frequently observed "dancing" of water droplets on a hot skillet is due to film boiling. This "dancing" behavior and the fact that droplets can last longer periods of time on hotter surfaces (T ≥ $T_{Leidenfrost}$) is known as the *Leidenfrost effect* [34]. The Leidenfrost effect has long been studied for room temperature liquids on flat surfaces [35,36] and more recently for cryogenic fluids [32]. It is not known how the

dynamics of the vapor layer are affected when a film boiling droplet is placed on a structured surface like that of our ratchets.

For our system, whose only energy source is the thermal gradient, it is conceivable that the observed motion could result from (1) the temperature gradient alone, (2) the dynamics of the vapor layer, or (3) both effects combined. We hypothesize that the existence and dynamics of the vapor layer are essential to the ability of the ratchet to induce droplet motion, and consequently droplets of any liquid in the film boiling regime will undergo motion, while droplets below the Leidenfrost temperature will not.

In our system, there is no gradient in surface chemical composition, and the only temperature gradient present is perpendicular to the direction of motion. Although some of the effects mentioned above, such as Marangoni flow, may play an important role in the behavior of the nitrogen droplets, the previous studies do not provide adequate explanation. The ratchet mechanisms currently used to move droplets are also unable to provide an explanation, since we are not applying any electric field or other external oscillatory force. In particular, no ratchet using a temperature gradient perpendicular to the direction of motion as its source of non-equilibrium has been studied. Therefore, we consider the observed behavior to be a novel phenomenon, and with this research attempt to understand its origin.

MATERIALS AND METHODS

The experiment setup is shown in Figure 8. During data collection, a ratchet is placed parallel to the edge of an adjustable table. We use ratchets with various periods, depths,

and angles (see Figure 9), as well as two materials (brass and Plexiglas). Table 1 lists the

ratchets used in the experiments.
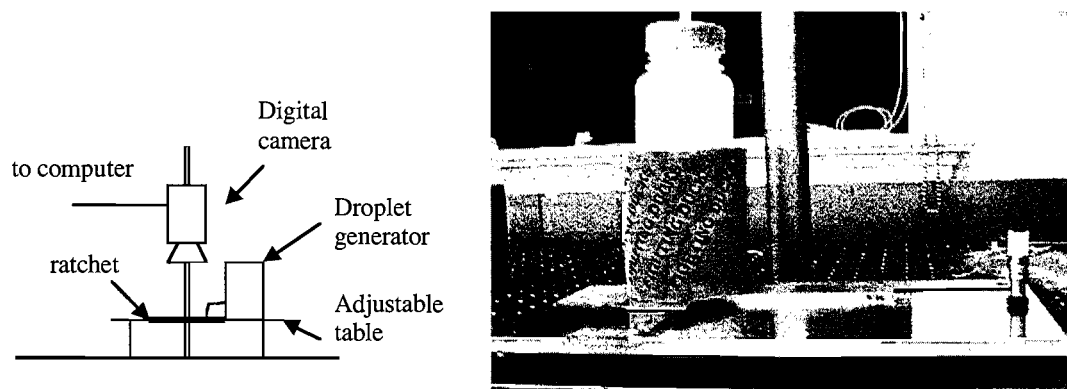
Figure 8: Experiment setup shown in (a) a schematic diagram and (b) an actual image. The ratchet is place on an adjustable table, which can be tilted to an incline. The motion is recorded from above using a digital video camera.

Figure 9: Schematic diagram of a ratchet. The preferred direction of motion is to the right. We use ratchets with various sawtooth periods (L), depths (d), and angles (α), as well as two materials: brass and Plexiglas (see Table 1).

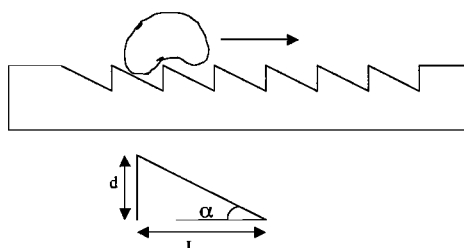**Table 1**: Specifications of the ratchets used in the experiments.

The letter M stands for metal (brass) and P for plastic (Plexiglas). Ratchet M-08 is the same as M-07, except it has been bead-blasted to increase roughness. M-09 is the symmetric ratchet shown in Figure 14.

	period, L [mm]	depth, d [mm]	angle, α [deg]
M-01, P-01	1.5	0.2	7.59
M-02, P-03	1.5	0.1	3.81
M-03	1.5	0.5	18.43
M-04	1.5	0.3	11.31
M-05	1	0.13	7.59
M-06	0.5	0.06	7.59
M-07	2	0.26	7.59
M-08	2	0.26	7.59
M-09 (Sym)	1	0.067	7.59

We level the adjustable table by placing droplets onto the smooth surface, and adjusting the three built-in screws until the droplets do not accelerate in any direction. The table can be placed at an incline, θ, by adjusting the screw at one end. The displacement, Δa, from the horizontal position can be determined using a scale with micrometer resolution on the screw, and converted to the angle of incline, using the relation:
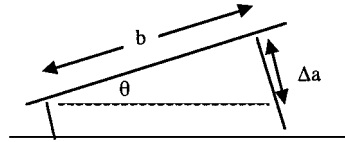
$$\theta = \arctan\left(\frac{\Delta a}{b}\right)$$

where b is the length of the table. The determination of level is accurate to about ± 0.3 mm, which corresponds to an uncertainty in all measured angles of ± 0.001 radians. The

uncertainty is determined by adjusting the incline of the table until it is clearly sloped uphill or downhill, evidenced by the acceleration of the nitrogen droplets. Due to experimental conditions, the table was re-leveled for each data set, meaning that each set of data is taken at a slightly different "zero" mark. The uncertainty in the determination of level is the dominant source of uncertainty for all angles measured, but is a larger relative effect for smaller angles. In the future, we hope to use test runs of droplets on flat brass in multiple directions to determine the actual angle of our "level" from later analysis of the acceleration. We could then adjust all measured angles accordingly.

Liquid nitrogen droplets are generated using the device illustrated in Figure 10. The device is required since other methods of droplet production, such as drops generated using a syringe, are unsuccessful due to freezing caused by the extreme low temperature, and the expansion of the evaporating gas. The design is motivated by a more sophisticated apparatus used by Chandra and Aziz [32]. A small, bent stainless steel tube of outer diameter 1.6mm is inserted into the container near the bottom. The tube is 1.5 inches in horizontal length, with a vertical section of 0.5 inches. At the bend, a small hole (0.5 mm diameter) is drilled through the outer wall of the tube. Nitrogen is placed into a 500ml polyethylene wash bottle, which is insulated using a typical consumer can insulator. Once the container and tube are cooled sufficiently, liquid will begin to flow through the tube and out of the small hole in the bend. The nitrogen then flows down along the outside of the tube, and collects at the tip. Once reaching a certain size, the droplets fall due to gravity. The standard size droplet produced is fairly consistent, at a radius of ~1mm. Larger droplets are formed by forcing the nitrogen to accumulate between the surface and the tip.

We also tested for the phenomenon with two other liquids, water and ethanol, at surface temperatures (> 280°C) that put the droplets in the film boiling regime. The ratchet (M-06) is heated by placing it on a Thermolyne hot plate. The temperature of the ratchet is measured using a thermocouple. Droplets of water and ethanol are generated using a syringe with a tip of inner diameter 2mm, which produce droplet radii of ~ 2mm.
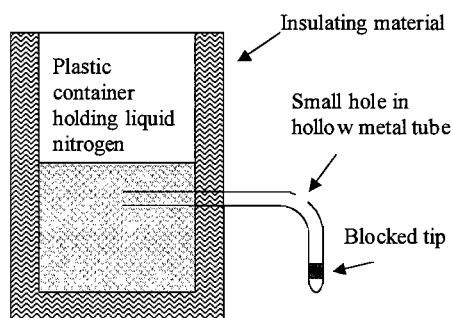
Figure 10: Droplet generator. Liquid nitrogen flows out of small hole in the bend of the metal tube. The nitrogen then runs down the side of the tube and accumulates at the tip until heavy enough to drop off.

Depending on the specific experiment, droplets are either released directly onto the ratchet near zero velocity or given various initial uphill or downhill velocities. To generate the initial velocities, droplets are released onto a simple aluminum plate used as a ramp. The ramp is tilted at various angles to produce the desired initial speeds.

The motion of the droplets is recorded from above using a digital video camera with a sampling rate of 30 frames per second. A millimeter resolution ruler is filmed next to the ratchet in order to create a scale. The movies are directly imported onto a computer using the program iMovie. Subsequently, position-versus-time data is obtained using VideoPoint software to manually track the motion of droplets on a frame-by-frame basis. Velocity and acceleration data are obtained by differentiating the position data obtained from VideoPoint using the following formulas:

$$v(t_n) = \frac{\Delta x}{\Delta t} = \frac{x(t_n) - x(t_{n-1})}{t_n - t_{n-1}}$$

$$\bar{v}_{2m+1}(t_n) = \frac{1}{2m+1} \sum_{j=n-m}^{n+m} v(t_j)$$

$$a(t_n) = \frac{\Delta \bar{v}}{\Delta t} = \frac{\bar{v}(t_{n+2}) - \bar{v}(t_{n-2})}{t_{n+2} - t_{n-2}}$$

where $\bar{v}_{2m+1}(t_n)$ is the average of 2m+1 velocity values, and $a(t_n)$ is the acceleration averaged over five velocity values in order to smooth out fluctuations created by scatter in the data. Scatter is created during the data acquisition process where a judgment must be made in choosing the center of the droplet on each frame, and the accuracy of this choice is limited by image resolution. The number of values over which to average was determined by balancing the desire to smooth out the fluctuations resulting from the data acquisition process and the requirement not to average out physically significant fluctuations.

RESULTS AND DISCUSSION

Phenomenological Description

By placing liquid nitrogen droplets on ratchet-like surfaces, it was observed that they move in a preferred direction relative to the asymmetry (to the right in Figure 9). Droplets released onto the ratchet at near zero velocity accelerate, and for small inclines (~2 degrees) this acceleration allows droplets to climb uphill. A series of experiments were designed and performed in order to explore these observations further. Our objective was to determine the nature of the ratchet-produced force, and in particular its

dependence on the dimensions of the sawtooth potential. During our attempts to determine the dependence of sawtooth dimension, we discovered that the net force on the droplet had a velocity dependent component.

Sawtooth Dimensions

In order to see how the strength of the force produced depends on the different sawtooth dimensions, we attempted to compare the maximum incline at which droplets are still able to climb for each ratchet. The critical angle is the incline at which the force produced by the ratchet surface equals the gravitational force. Because the gravitational force is known, we would also be able to extract an estimate for the force produced at this incline. Initial attempts to perform this experiment, while keeping the droplet size fixed, were not successful. We were not able to resolve differences between the ratchets, but obtained a general impression that droplets can climb inclines on the order of a few degrees. Various problems hindered our ability to determine more precise values. Although these problems have been individually addressed, as described below, this experiment has not been repeated due to the pursuance of more recent results.

First, various portions of the ratchet surface appeared to behave differently. The inconsistencies in the ratchet are believed to be due to oxidation and dirt accumulating on the surface. To eliminate this problem, the ratchets were cleaned and polished, a procedure that will be repeated as needed in future research.

Second, the droplet size used did not work as well, or at all, on some ratchet dimensions. To determine the impact of droplet size on the existence and strength of the observed behavior, a simple experiment was designed to find the relationship between the ratchet dimensions, droplet size, and the strength of the resulting acceleration. Various

droplet sizes were placed on our ratchets with the table leveled, and a numerical score indicating the strength of the effect recorded. The droplet diameter was determined by visual observation. Comparing droplet diameter to ratchet period showed that the force was strongest when the droplet covered at least one period. Droplets slightly smaller experienced a reduced force, while droplets with a diameter less than ~2/3 the ratchet period no longer moved. This result could be made more accurate using a device with the ability to consistently produce various droplet sizes, the diameter of which could be measured from a movie using VideoPoint.

Third, it was difficult to determine a cutoff for when the droplets were climbing, due in part to the two preceding problems. As a revision of the previous experiment, we attempted to determine the maximum incline *at which the ratchet force was still observed*. We hypothesized that the critical incline would equal the angle of the sawtooth grooves for each ratchet, since at this incline the "downhill" part of the sawtooth becomes horizontal with respect to gravity (see Figure 11).
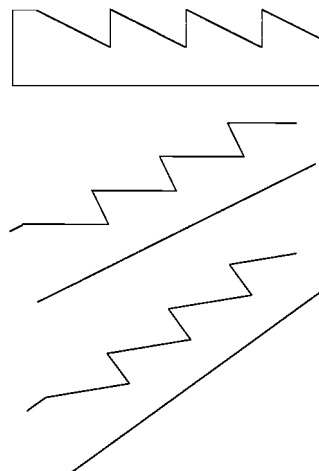
Figure 11: Schematic diagram of a ratchet tilted at various inclines. (a) The ratchet on level. (b) The ratchet tilted to an incline equal to the angle of the sawtooth slope. At this point the "downhill" portion of the sawtooth is horizontal. (c) The ratchet tilted even steeper, the "downhill" portion is now actually uphill.

To detect if the ratchet force was present at a given angle, we designed a new experiment in which the motion of a droplet on the ratchet surface was compared with a "test droplet" on a flat surface (see Figure 12). In successive experiments, each surface was placed at the same incline and droplets were released with the same initial uphill velocity. At each incline, we compared the distance traveled by the droplets on each surface. Our assumption was that if the ratchet force was acting on the droplet, it should gain energy and be able to glide uphill further than the "test droplet".
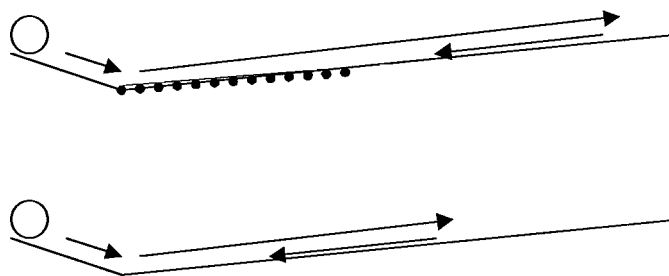
Figure 12: Comparison Experiment. Each droplet is given the same initial velocity (determined by initial height) and the droplet is allowed to come to a stop due to gravity. In the top example, the droplet passes over a ratchet surface, while in the bottom the droplet glides only on a flat surface. If the ratchet is producing a force in its preferred direction (in this case uphill), the top droplet should glide further.

Based on this idea, we attempted to increase the incline until the droplets on both surfaces traveled the same distance, which would indicate a ratchet force of zero. However, the observed result was that for some initial velocities the droplet on the ratchet went a shorter distance than the "test droplet". Such a result indicates that, for these velocities, the force produced by the ratchet surface was in the downhill direction, opposite to the ratchet's specified direction of motion. While for other velocities, the droplets clearly experienced an upward force, given that they accelerated as they climbed uphill. We still need to verify the maximum angle at which the ratchet force is observed, however we decided to pursue these new observations, which we believe to be a more enlightening method for learning about the observed behavior.

Velocity Dependence

To probe this velocity dependent behavior further, droplets were given a spectrum of both positive and negative initial velocities, and the resultant motion was recorded. By plotting the velocity of each droplet versus time, it was observed that a steady-state

velocity exists for each ratchet (see Figure 13). Droplets introduced to the ratchet surface slower or faster than this velocity either accelerate or decelerate to reach the steady-state velocity. For small inclines, droplets released with downhill velocity were able to turn around and climb uphill.

In some cases, droplets with both positive and negative initial velocities approach the same terminal velocity. However, on some ratchets we have observed more than one steady-state velocity. In addition, each terminal velocity value appears to have a certain width. Examples of various terminal velocity behaviors are shown in Figure 13. Notice the short time (< 0.5 s) before terminal velocity is reached. A summary of the apparent terminal velocities for all of the brass ratchets is given in Table 2.

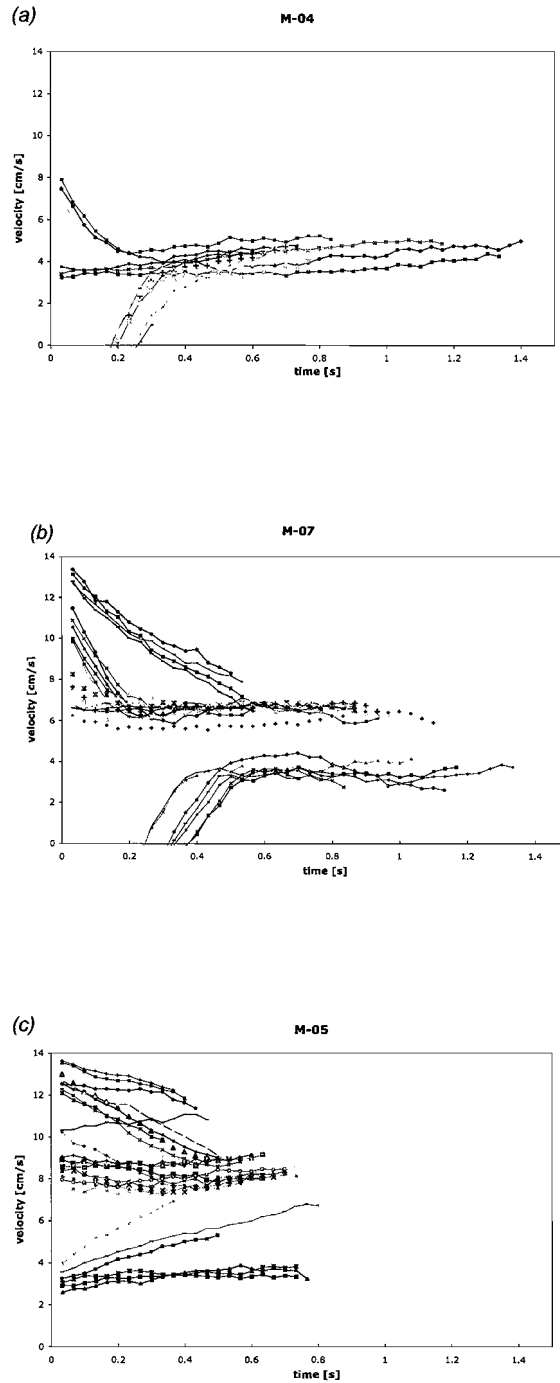**Figure 13**: Examples of the terminal velocity behaviors observed on different ratchets, each at zero incline. (a) All droplets reach a fairly consistent range of terminal velocities. (b) Droplets launched with positive or negative initial velocities reach distinct terminal velocity ranges. (c) Droplets reach what appear to be several separate terminal velocities, depending on initial velocity.

Table 2: The terminal velocities reached by droplets on each ratchet.

The row headings v+ and v- indicate droplets launched with velocities above or below the terminal velocity, respectively. The two levels within each row are divisions into what may be two distinct regions of terminal velocity ranges.

Ratchet	M-01	M-02	M-03	M-04	M-05	M-06	M-07	M-08
v-	~4.0 – 6.0	?	~2.5 – 3.5	~3.3 – 5.0	3.5		~3.0 – 4.0	~3.0 – 4.0
[cm/s]			5.7		~7.5 – 9.0	~8.0 ?		
v+	~5.0	4.0 ?		~3.3 – 5.0				No data
[cm/s]	7.0		5.7		~7.5 – 9.0	~8.0 ?	~6.0 – 7.0	

We have experimentally determined that film boiling nitrogen droplets placed on asymmetric ratchet-like surfaces accelerate in a preferred direction relative to the asymmetry. The droplets are able to climb inclines up to ~2 degrees, depending on the specific ratchet. So far, we have not been able to resolve the dependence of the acceleration on the sawtooth dimensions. In our attempts to determine this relationship, we discovered an interesting behavior of the droplets. Droplets placed on the ratchet surfaces quickly (< 0.5 seconds) reach a terminal velocity. In order to study this behavior in detail, we isolated various components of the system. We first analyzed droplet motion of flat brass surfaces, and subsequently on symmetrically and asymmetrically grooved surfaces, the results of which are provided below.

Droplets on Flat Surfaces

We originally hypothesized that the observed behavior of the droplets may be due to the expanding vapor beneath the droplets, which could somehow provide a "kick" to the droplets. For a stationary droplet on a level surface, the expanding vapor will flow outward equally in all directions. However, by tilting the surface and thereby creating

motion of the droplet, we thought that the vapor might escape more easily from the "rear" of the droplet, perhaps causing forward acceleration. Because our droplets see a downhill slope for each period of the ratchet (see Figure 9), any "kick" present on a flat surface could be responsible for the acceleration of the droplet.

To test this idea, we tracked the motion of nitrogen droplets on a flat brass surface at various inclines. The droplets were released onto the aluminum ramp to create an initial uphill velocity, after which they turned around due to gravity. Assuming that gravity was the only force acting on the droplet, we would expect the velocity to change linearly with time, at a rate given by the corresponding constant gravitational acceleration ($g\sin\theta$). A plot of droplet velocity, $\bar{v}_9(t_n)$, is shown in Figure 14 for an incline of 0.004 radians (0.23 degrees). The figure also shows data from our symmetric and ratchet surfaces, which will be discussed later.
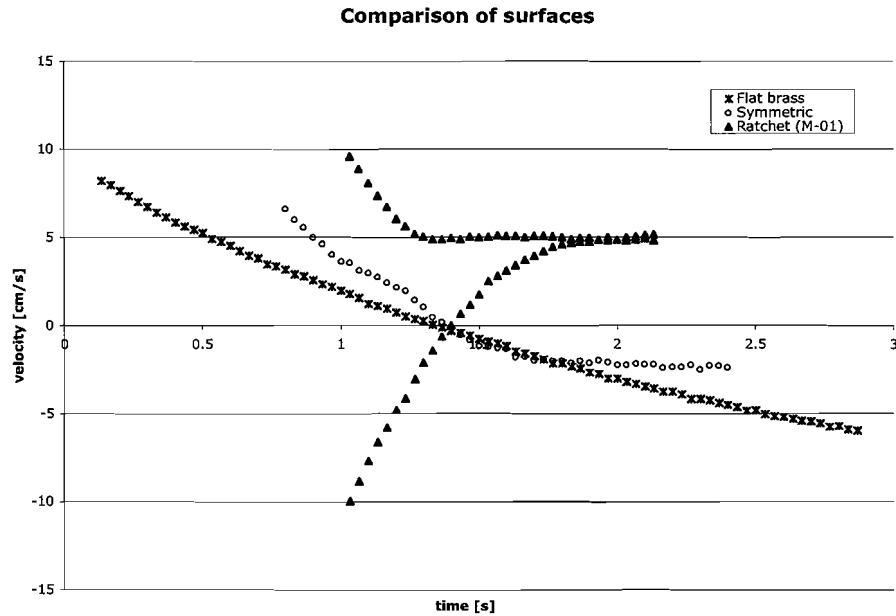

Figure 14: Comparison of the velocity evolution over time for our three types of surfaces: flat, symmetrically ridged, and ratchet (asymmetrically ridged). The flat and symmetric data are at an incline of 0.004 radians, while the ratchet data is at an incline of 0.006 radians.

Based on the curvature of the $\bar{v}_9(t_n)$ plot, we suspected the presence of a velocity

dependent drag force acting on the droplet, in addition to the constant gravitational force.

A velocity-dependent force is equivalent to a velocity-dependent acceleration, and for our

purposes acceleration is easier to work with. Figure 15 shows acceleration, $a(t_n)$, as a

function of velocity, $\bar{v}_9(t_n)$, for a droplet on flat brass.
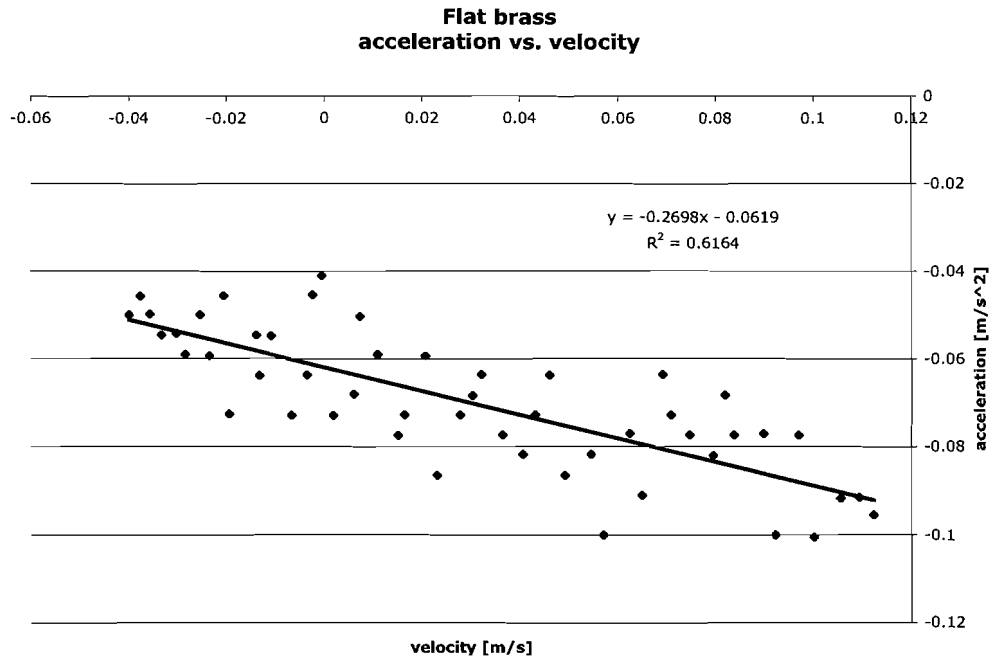
**Flat brass
acceleration vs. velocity**

Figure 15: Acceleration as a function of velocity for a nitrogen droplet
on a flat brass surface (incline = 0.007 radians).

The linear nature of the velocity dependence indicates a possible drag force

directly proportional to v, so that the net force could be written as:

$$F_{net} = -F_{drag} - F_{constant} = -\beta v + F_{constant}$$

where β is the drag coefficient, and $F_{constant}$ is the sum of any constant forces. This is

consistent with the fact that drag at low Reynolds numbers is usually linear in the

velocity. To solve the above equation for $v(t)$ we write (assuming a constant mass):

$$m\frac{dv}{dt} = -\beta v + F_{constant}$$

which can be easily solved (see Appendix) to obtain:

$$v(t) = \left[v(0) - \frac{F_{constant}}{\beta}\right]e^{-\frac{\beta}{m}t} + \frac{F_{constant}}{\beta}$$

$$= \left[v(0) - \frac{a_{constant}}{\beta/m}\right]e^{-\frac{\beta}{m}t} + \frac{a_{constant}}{\beta/m}$$

Equation (1)

Velocity versus time data for multiple droplets at various inclines were fit using Equation (1), with parameters β/m, $a_{constant}$, and $v(0)$. Either $\bar{v}_3(t_n)$ or $\bar{v}_9(t_n)$ data was used, depending on the length of the data set. The results for $a_{constant}$, normalized to gravitational acceleration, are shown in Figure 16.
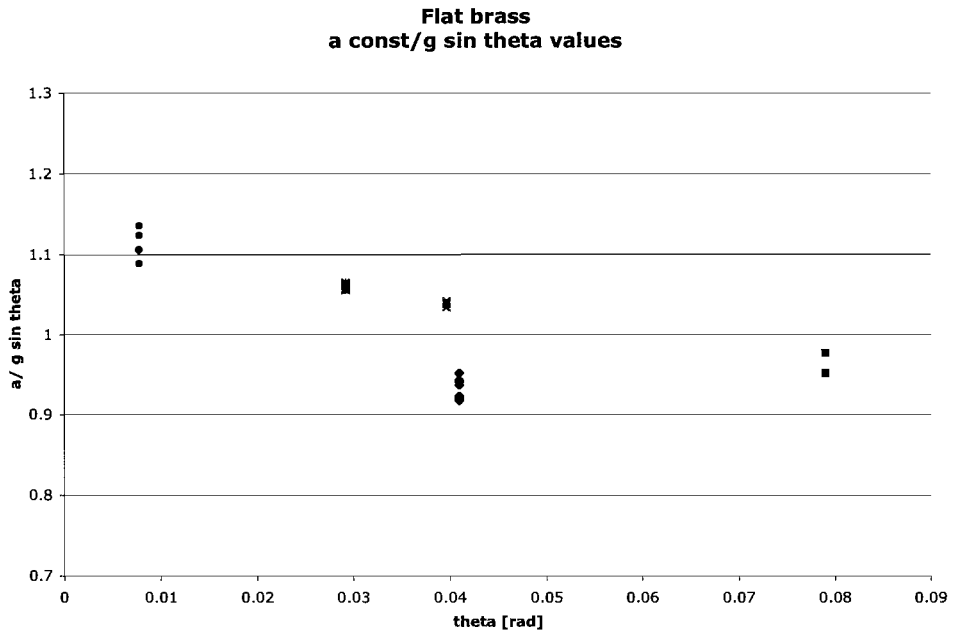

Figure 16: Results for $a_{constant}$ of a nitrogen droplet on flat brass, obtained from fitting velocity versus time data to Equation (1). The results have been normalized to the corresponding gravitational acceleration for each incline.

The current results show that all of the $a_{constant}$ fit values obtained using Equation (1) lie within 15% of the expected value, with the majority within <10%. The small spread for each data set indicates that Equation (1), although not proven the correct model, at least provides consistent results. Also, the close agreement with gravitational acceleration indicates that any "active" acceleration of the nitrogen droplet on flat surfaces would be small. Although there appear to be a few trends (the presence of some values above 1, and the possible linear decrease with incline), these cannot yet be confirmed due to the uncertainty in the determination of level, which affects all calculated angles. The uncertainty in the angle measurement would also have the largest influence on the smallest angles of incline, possibly accounting for the increased deviation from the expected value at small inclines. A method for reducing the uncertainty in the angle of incline is described in the above section.

The results for β/m values for the same fits are shown in Figure 17. Despite the scatter, we can extract an estimate for the ratio of $\sim0.25 - 5.0$ s^{-1}.
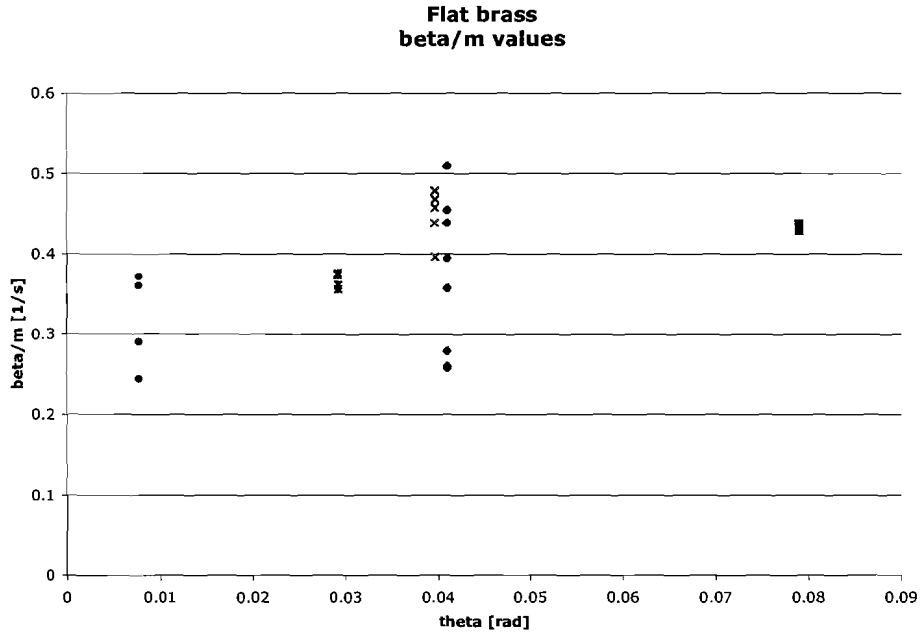
**Flat brass
beta/m values**

Figure 17: Results for the drag coefficient on flat brass obtained from fitting velocity versus time data to Equation (1).

These data have a larger spread than the results for $a_{constant}$. This could be due to multiple factors. First, the initial mass varies between droplets and the droplet mass changes over time. Both mass fluctuations would affect the β/m ratio. It is possible that fluctuations in mass reach ~10% or more, which could account for a large portion of the spread. Another possibility is that the data sets we have are not that curved (due to the small value of β/m), and thus the fits are highly sensitive to any fluctuations in the data. For example, the largest spread is present for an angle (0.04 rad) where $\bar{v}_3(t_n)$ was used due to the short data set. This issue could be resolved in the future by taking longer data sets.

Now that we have obtained a numerical value for β/m, we can compare our value to common types of drag forces the droplet may be experiencing. Using Stokes' Law for laminar flow, we can estimate the drag coefficient expected from air resistance.

The drag force is given by $F = 6\pi\eta rv$, so that $\beta_{Stokes} = 6\pi\eta r$, where η is the viscosity of air and r is the radius of the droplet. We obtain a value of:

$$\beta_{Stokes} = 6\pi\eta r$$

use $\eta = 17.9 \ \mu Pa \bullet s$
$r = 1mm$
$\rho = 0.807 g/mL$
$V = \frac{4}{3}\pi r^3 = 0.0042 cm^3$
$m = V\rho = 3.4 \bullet 10^{-6} kg$

$$\beta_{Stokes} = 3.4 \bullet 10^{-7} kg \bullet s^{-1}$$
$$\frac{\beta_{Stokes}}{m} = 0.01 s^{-1}$$

which is an order of magnitude lower than the experimentally determined drag coefficient. This suggests air resistance is not the primary source of drag.

Another possible source of drag is viscous drag due to the motion of the droplet above the vapor layer. For a simple estimate, we assume that the gas directly beneath our droplets is moving at the speed of the droplet (this is zero velocity with respect to the droplet), while the gas at the brass surface is stationary. We neglect the (possibly significant) outward flow of the vapor beneath the droplet. The viscous drag force is then given by $F = \pi r^2 \eta v/h$, where η is the viscosity of the nitrogen vapor layer (chosen at T = 200 K), h is the height of the vapor thickness, and r is the radius of the drop bottom. Because our droplets flatten slightly, this radius used here is larger than used above. We use a vapor thickness of 50 micrometers, an estimate based on the experimental results of Chandra and Aziz [32]. Calculating, we have:

$$\beta_{Viscous} = \frac{\pi r^2 \eta}{h}$$

use $r = 1.5$ mm

$\eta = 13 \ \mu Pa \cdot s$

$h = 50 \mu m$

$\beta_{Viscous} = 1.4 \cdot 10^{-6} kg \cdot s^{-1}$

$\frac{\beta_{Viscous}}{m} = 0.41 s^{-1}$

which is on the order of the observed value, indicating that viscous drag from the vapor layer is likely the key source of drag experienced by the droplets on flat brass.

The results obtained from analysis of position versus time data for nitrogen droplets on flat brass surfaces show that the net force on the droplets is the constant acceleration expected from gravity, with the addition of a slight drag force that slows the droplet. The results do not support the idea of acceleration from evaporation that might give the droplet a "kick." We were, however, able to develop a model to describe the forces acting on the droplet and determine a numerical value for the drag coefficient, which is on the order of the expected value from viscous drag due to the vapor layer.

Droplets on Symmetrically Structured Surfaces

In order to verify that the asymmetry of the sawtooth shape is a requisite for motion, we designed and tested a symmetrically structured surface (see Figure 18). The dimensions of the symmetric surface (the period and the angle of the slopes, α) were chosen to be similar to the dimension of our asymmetric ratchets (see Table 1). We hypothesized that the novel behavior of the droplets would not be observed on the symmetric surface when placed at zero incline. We also suspected that the behavior might be observed when the

symmetric surface was placed at a high enough incline, since as the surface is tilted it

becomes increasingly asymmetric with respect to the horizontal (see Figure 18 (b)).
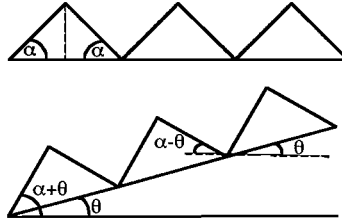

Figure 18: Schematic diagram of our symmetric surface (a) on level
and (b) when placed at an incline.

A plot of velocity versus time for a droplet on the symmetric surface, as well as

on the flat brass surface and ratchet M-01, is shown in Figure 14. Preliminary

observations indicated that the "ratchet effect", if present on the symmetric surface, was

not evident. The droplets released with uphill velocity simply turned around and

accelerated downhill, while on the asymmetric ratchets these droplets climb uphill. The

strong curvature of the $\bar{v}_9(t_n)$ plot for the symmetric surface appears to be due to a drag

force significantly stronger than that found on flat brass.

Using the same drag model we used for flat brass, the velocity versus time data

for the symmetric surface was fit using Equation (1). The results for $a_{constant}$, again

normalized to gravitational acceleration, are shown in Figure 19. The values for $a_{constant}$

on the symmetric surface lie within a small range ($< 10\%$) above or below the values

predicted from gravity. The precision of the data lends additional validation to the use of

Equation (1) as a reliable means for determining $a_{constant}$. The close agreement with the

expected value for all analyzed inclines indicates that there is no additional force due to

the ridges. This supports our hypothesis that droplets placed on the symmetric surface at

zero incline will not undergo directed motion. However, the results also indicate that the asymmetry due to tilting the surface is not significant enough to lead to droplet motion. This result suggests that the sharp asymmetry of our sawtooth pattern is essential to the behavior we have observed.
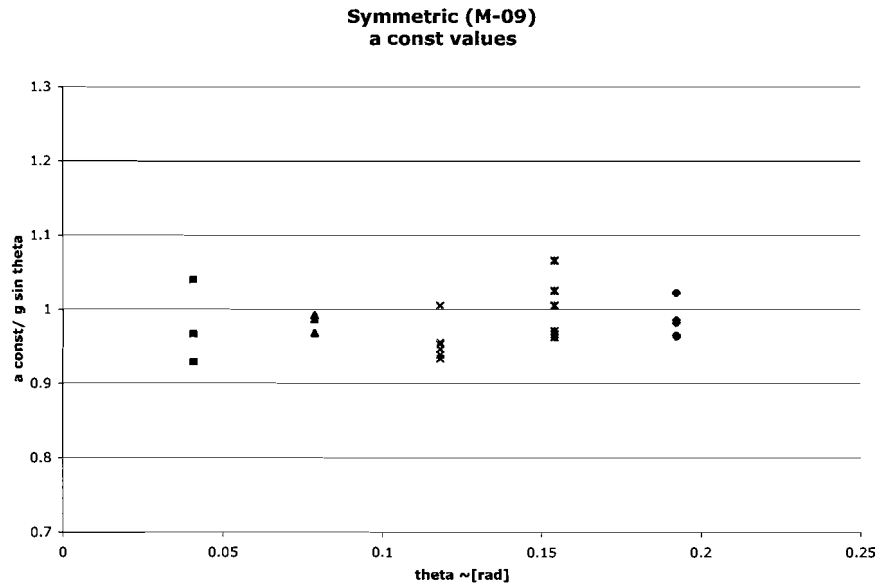

Figure 19: Results for the constant acceleration experienced by a nitrogen droplet on the symmetric surface, obtained from fitting position versus time data with Equation (1). The results are normalized to the corresponding gravitational acceleration for each incline.
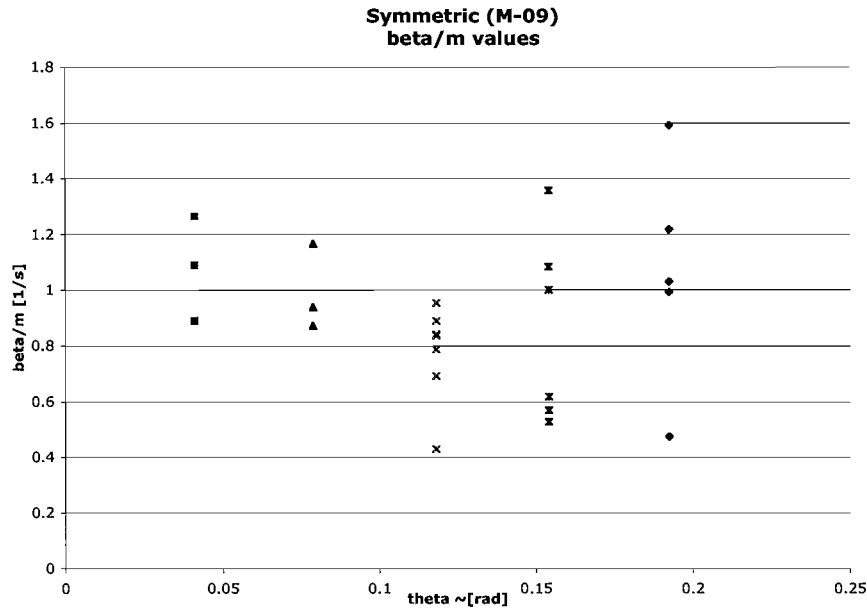
Figure 20: Results for the drag coefficient for the symmetric surface, obtained by fitting velocity versus time data with Equation (1).

The corresponding results for β/m are shown in Figure 20. Despite the large scatter, the values for the ratio are clearly larger than those calculated for flat brass. Most of the data points lie within a range of ~0.5 –1.3 s^{-1}. This is a large range, but still provides an estimate that can be used for comparison purposes. The large scatter is probably due to a number of factors, considering the possibly complex interaction of the droplets with the ridges in contrast to droplets on flat surfaces. Recall that for flat brass we obtained a range of ~0.25 – 5.0 s^{-1}. Thus, we can conclude that the presence of symmetric ridges roughly doubles the effective drag experienced by the droplet.

The increase in drag can be understood by visualizing the droplet on the symmetric surface, as in Figure 21. On a flat surface, the droplet will be at a fairly constant equilibrium height above the surface. On the symmetric surface, however, the droplet must bend around the surface, tending to cut-off the free flow of the gas,

restricting its flow to a smaller channel. The smaller effective channel height would lead to an increase in the amount of viscous drag.
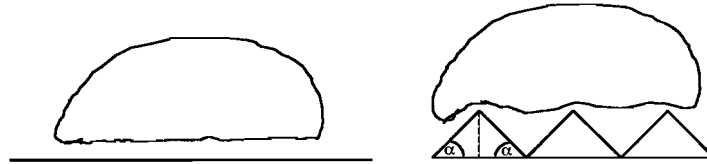

Figure 21: Schematic diagram of a nitrogen droplet on (a) a flat surface, and (b) the symmetric surface. On the flat surface, gas can flow through the channel of constant height. On the symmetric surface, the shape of the ridges and the droplet tend to cut off free flow, reducing the effective channel height.

Our analysis of the motion of droplets on symmetrically structured surfaces provided results similar to the flat brass case. We have shown that the acceleration can be divided into two components: (1) a constant downhill acceleration, and (2) a velocity-dependent drag acceleration opposing the motion of the droplet. In comparing the results for the constant acceleration with the expected value from gravity, we found close agreement, indicating that there was no "ratchet phenomena" of a directed force due to the symmetrically structured surface. Such a result indicates that sharp asymmetry is a requisite for the "ratchet phenomenon." We have also extracted a value for the drag coefficient, and determined that it is roughly twice as large as the drag coefficient found for droplets on flat brass.

Droplets on Asymmetric Ratchet Surfaces

To determine how the observed ratchet force depends on velocity, we wanted to compare the terminal velocities achieved at several inclines. By definition of terminal velocity there is no net acceleration, so the sum of the non-gravitational (ratchet plus

drag) acceleration must be equal in magnitude but opposite in direction to gravity. If we

denote $a_{other} = a_{ratchet} + a_{drag}$, we then have the relation $a_{other}(v_{term}) = g \sin \theta$. A plot of the

net acceleration due to the ratchet surface at the terminal velocity, $a_{other}(v_{term})$, is shown

in Figure 22. The terminal velocity is obtained from velocity versus time plots for each
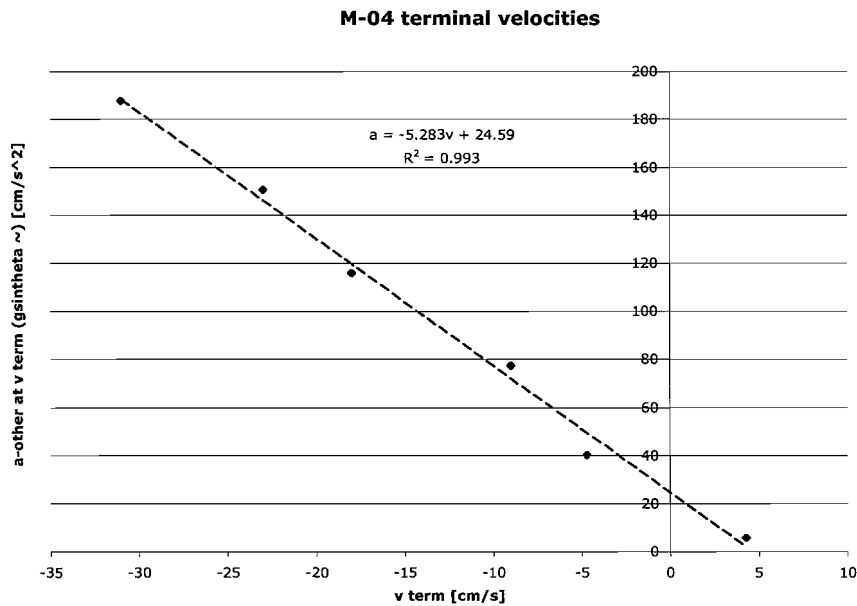
incline.

M-04 terminal velocities

Figure 22: A plot of terminal velocity as it varies with incline. To extract the acceleration produced by the ratchet surface (ratchet + drag), the terminal velocities are plotted versus g sin (theta) rather than the incline.

The linear nature of the plot indicates that the presence of a force proportional to

velocity. However, the non-zero force at a velocity of zero indicates a velocity

independent force is also present. Assuming the ratchet asymmetry produces the velocity

independent force, the data can be modeled using the equation:

$$a_{other} = a_{drag} + a_{ratchet} = -\frac{\beta}{m}v + a_{ratchet} \qquad \text{Equation (2)}$$

where $a_{ratchet}$ is the constant acceleration exerted by the ratchet (due to the asymmetry).

A linear fit using Equation (2) gives a result of $a_{ratchet} \approx 25$ cm/s^2 and $\beta/m \approx 5.3$ s^{-1}.

To verify the consistency of these values in relation to those obtained for flat brass and symmetric surfaces, the ratchet data was also fit using Equation (1). If we assume a constant ratchet force, as in the above analysis, we expect to have $a_{constant} = a_{ratchet} - |a_{gravity}|$ in Equation (1). The results for $a_{ratchet} = a_{constant} + |a_{gravity}|$ are shown in Figure 23.
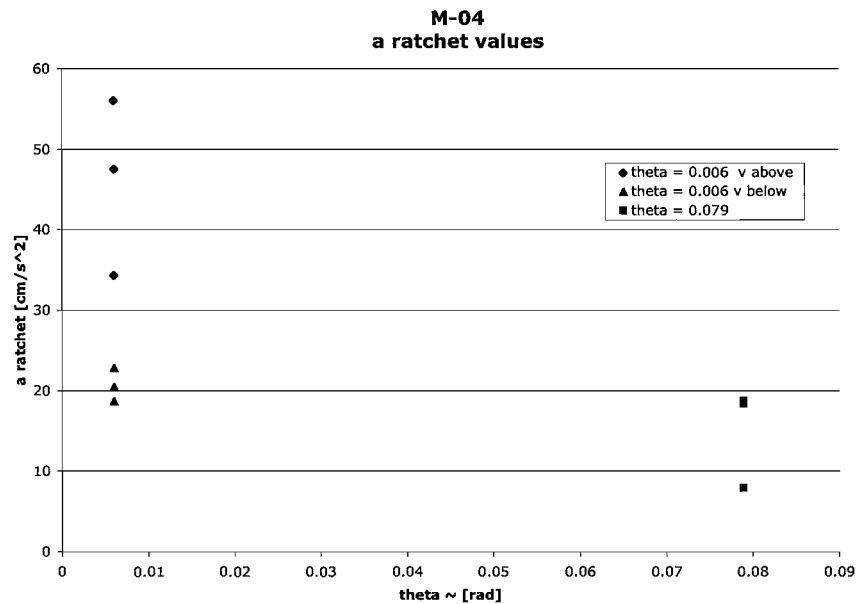
Figure 23: The ratchet acceleration for M-04 at various inclines, obtained from fitting velocity versus time data using Equation (1). For 0.006 rad: the data represented by triangles is from droplets released below terminal velocity, while that represented by diamonds is from droplets released above terminal velocity.

Due to the limited amount of data analyzed so far, it is hard to draw many conclusions. However, there are some observations that can be made. First, for two of

the three data sets analyzed (triangles and squares in Figure 23), the calculated ratchet

force is close to that obtained from the plot of terminal velocity versus a_{other}. Recall that

the value previously calculated was $a_{ratchet} \approx 25$ cm/s^2, while here the majority of points lie

within $18 - 25$ cm/s^2. The results for β/m are shown in Figure 24. We see that the

same data sets that match the earlier results for $a_{ratchet}$ also match the earlier result for

β/m reasonably well, with all but one value falling within the range of $\sim 5.0 - 5.5$ s^{-1}

(above we obtained ~5.3 s^{-1}). The third data set (diamonds) yields values about a factor

of two larger for both a_{other} and β/m. It is interesting to note that these droplets were

introduced to the system at velocities higher than the terminal velocity, and therefore

experienced negative acceleration. We had previously observed by eye that such

"braking" appeared much stronger than the "speeding-up" process. Although these data

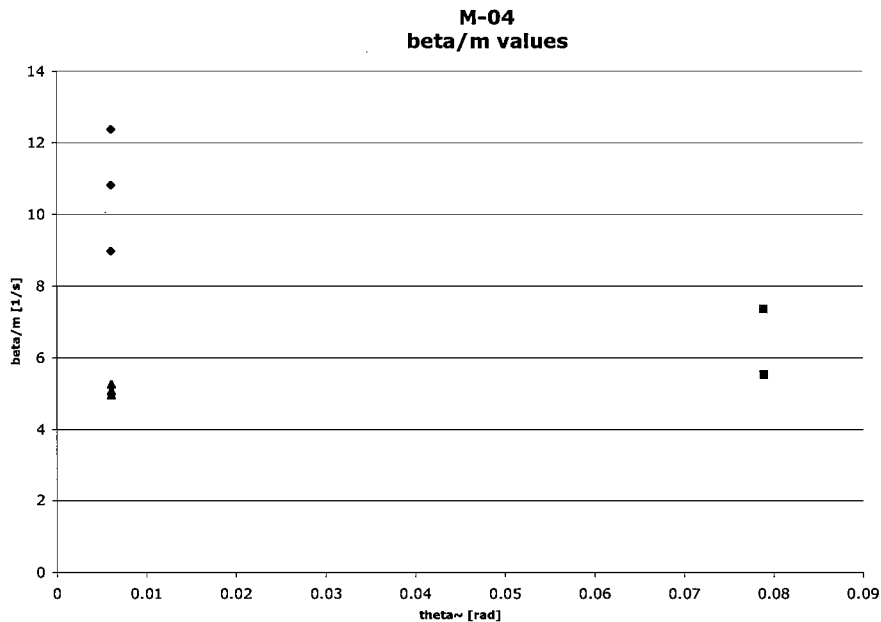seem to verify our observations, the physical reason for this behavior is not yet known.

Figure 24: Results for the drag coefficient for droplets on ratchet M-04. See Figure 23 for details.

In addition to testing liquid nitrogen droplets on various brass ratchets, we also tested nitrogen droplets on several plastic ratchets, as well as two other liquids on one of our brass ratchets. Figure 25 shows a comparison of droplet velocity on brass and plastic ratchets of the same sawtooth dimensions (M-01 and P-01). The droplets on the plastic clearly reach a much higher terminal velocity – 9 cm/s compared to 6 cm/s for nitrogen droplets on brass. We are currently investigating the possible influence of material properties (such as heat conductance and surface roughness) on the resultant motion of the droplets.

Comparison of Surface Materials
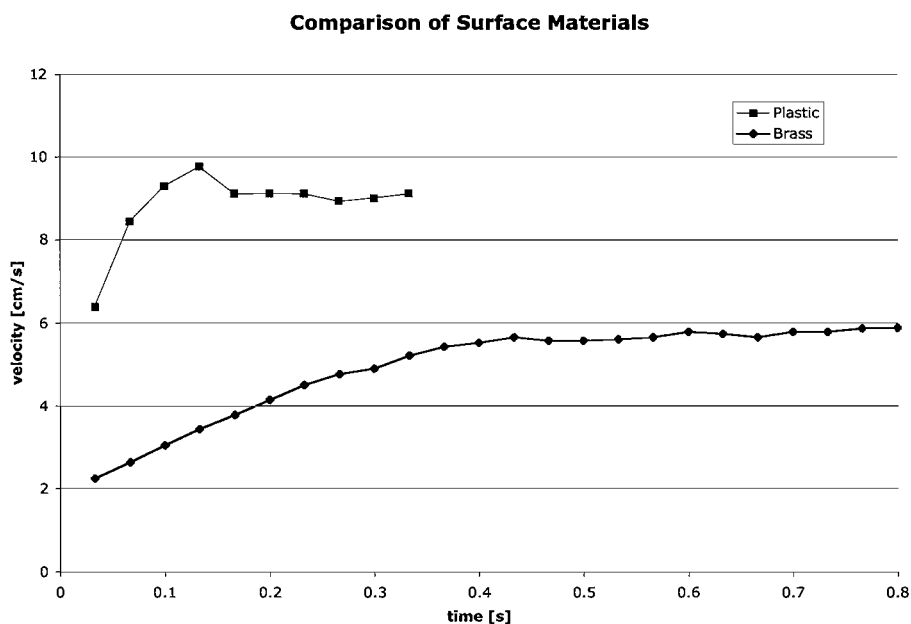
Figure 25: A comparison of the velocity evolution on brass (M-01) and Plexiglas (P-01) ratchets. The two ratchets have the same sawtooth dimensions.

Figure 26 shows a comparison of the three liquids: nitrogen, water, and ethanol. The water and ethanol data were obtained at a surface temperature of 410 C, while the nitrogen data was obtained on a room temperature (~20 C) surface. The water and ethanol droplets were larger (r~2mm) than the nitrogen droplets (r~1.3mm), due to the

method of production. We first note that the "ratchet behavior" (droplets experiencing a directed ratchet force) is observed for each liquid above its Leidenfrost temperature, supporting the hypothesis that film boiling is a sufficient condition for directed motion. We know that room temperature liquids do not exhibit this behavior on room temperature surfaces, but must still verify that the cutoff temperature for a ratchet force is the Leidenfrost temperature. Second, we see that the water droplets behave similar to the liquid nitrogen droplets, approaching roughly the same terminal velocity (~ 6 cm/s). The ethanol droplets experience a larger acceleration (by a factor of ~ 2), and appear to be heading for a much larger terminal velocity, perhaps near 15 cm/s.
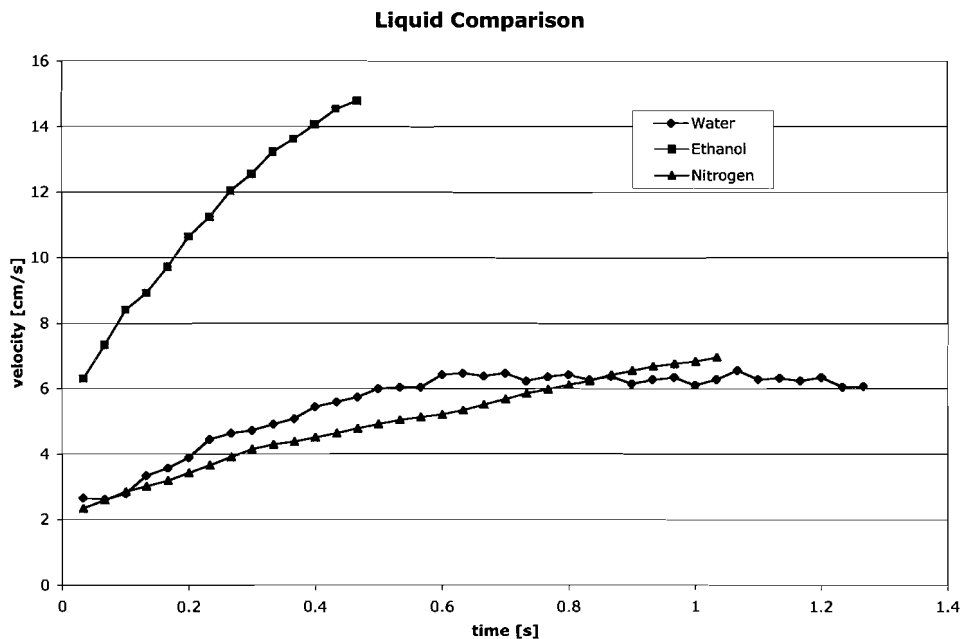
Figure 26: A comparison of the velocity evolution for various liquids on ratchet M-06 with no incline. The water and ethanol data were obtained for room temperature liquids on a surface temperature of 410C. The liquid nitrogen data were obtained for 77K nitrogen on a room temperature surface.

To compare the strength of the ratchet force and drag force on these three liquids, each data set was fit using Equation (1). The results are shown in Table 3.

Table 3: Results for the fits of the data for various liquids,
obtained using Equation (1).

	Nitrogen	Water	Ethanol
$a_{ratchet}$ (m/s^2)	~ 0.08	~ 0.25	~ 0.45
β / m (s^{-1})	~ 0.7	~ 4.0	~ 2.3

The values for the drag coefficient and the ratchet force for nitrogen are very low in comparison to our previous results for ratchet M-04. This discrepancy could be due the difference in sawtooth dimensions between the two ratchets. Assuming a constant force, the difference in the values for $a_{ratchet}$ would be enhanced by the variance in the mass between the nitrogen and the other liquids, which had radii about a factor of two larger. The much larger terminal velocity of the ethanol in comparison to water droplets appears to be due to both an increased ratchet force and a decreased drag force. Assuming that the vapor layer is critical to the motion, the variation in drag force may be due to a difference in the viscosity of the gases or the height of the vapor layers, while the change in the "ratchet force" may be a consequence of varied evaporation rates or surface tensions of the liquids. We are currently researching these possibilities.

We hope to obtain more data with several liquids and surfaces to determine the dependence of the ratchet force on various parameters. Once we know what properties the force depends on, we will be in a position to formulate a model for the cause of the "ratchet force."

CONCLUSION

We have presented a novel phenomenon by which film boiling droplets are made to move in a preferred direction on an asymmetrically structured "ratchet" surface. We have given a phenomenological description of the behavior. Droplets placed on the ratchet surfaces experience an acceleration that brings them toward a terminal velocity. We have shown that the "ratchet force" (any constant force other than gravity) is effectively zero on both a flat brass surface and a symmetrically structured surface across a range of inclines. Thus sharp asymmetry is essential to the existence of the observed phenomenon. Assuming that the ratchet surface produces a constant "ratchet force" in combination with a drag force proportional to the velocity of the droplet, we have determined estimates for the corresponding ratchet acceleration and drag coefficient. However, we do not currently have an explanation for the existence of more than one terminal velocity on a given ratchet (or, similarly, the disparity between results obtained for droplets with different initial velocities).

We have demonstrated that the behavior occurs for each of the three liquids tested, above their respective Leidenfrost temperatures. We have also shown that both liquid and surface material properties can strongly affect the motion of the droplets, although we have not drawn conclusions about the origin of these effects. We are in the process of investigating material parameters we believe could be of importance.

Recently, we have observed that nitrogen droplets incident on a step with a rough edge (such as the edge of a piece of masking tape on a metal plate) will accelerate strongly when passing over the edge, toward the region of higher elevation. This may indicate that the sharp edge of the sawtooth profile is the location where the acceleration

takes place on the ratchet. We are currently pursuing this observation in hopes of isolating the process responsible for the directed force on the droplet. By studying the simpler case of one step, we will be able to more easily determine the influence of all parameters of interest, including sawtooth dimensions, liquid and surface properties, and temperature.

Clearly, more experiments must be completed before we have a comprehensive understanding of the behavior we have presented. In addition to our ongoing experiments, we are working on developing physical explanations for the observed phenomena. Combining theoretical and experimental approaches, we hope to derive the equations of motion for the droplets.

ACKNOWLEDEMENTS

GLOSSARY

Contact angle – The angle between a solid surface and the tangent line to the edge of a droplet.

Equilibrium – The state at which all evolution has ceased.

Film boiling – Boiling where a film of vapor separates the warm solid from the boiling liquid.

Gibbs free energy – In general, the amount of energy that must be externally supplied to create any system at constant pressure. **Interfacial** (or surface) **Gibbs free energy** is the amount of energy required to form a unit area of an interface between two substances (generalized surface tension).

Gradient – A smooth variation in a certain quantity, for example in temperature or chemical concentration.

Leidenfrost effect – The phenomenon that droplets last longer and "dance" on surfaces at or above the Leidenfrost temperature; also another term for film boiling.

Leidenfrost temperature – The minimum temperature to support film boiling; also the temperature at which the heat transfer to the droplet is a (local) minimum [33].

Macroscopic – Indicates a large length scale. In the context of gradients, indicates the gradient is present over the entire length of motion.

Marangoni effect – The flow of liquid due to a surface tension gradient [28].

Ratchet – a system utilizing disequilibrium and local asymmetry (local gradients) to generate large-scale motion.

Surface tension – The common term for the liquid-gas interfacial (or surface) Gibbs free energy. The force per unit length exerted (perpendicular to the surface) when the

liquid is contracted or expanded, or equivalently the amount of energy required to form a unit area of a liquid-gas interface [28].

Surfactant – ("Surface-active-agent") A long molecule with one hydrophobic and one hydrophilic end. This chemical structure attracts the molecule to interfaces (such as solid-liquid).

Thermal equilibrium – The state at which all objects in a system are at the same temperature

Thermocapillary flow – Marangoni flow induced by a temperature gradient.

Wettability – An indicator of how much a droplet will wet (or spread out on) on given surface. Wettability is determined by the interfacial Gibbs free energies of the substances present and is measured by the contact angle.

APPENDIX: DIFFERENTIAL EQUATION FOR DRAG MODEL

$$m\frac{dv}{dt} = -\beta v + F_{const}$$

$$\frac{dv}{-\beta v + F_{const}} = \frac{1}{m} \cdot dt$$

$$\int \frac{dv}{-\beta v + F_{const}} = \frac{1}{m}\int dt$$

$$\frac{\ln[-\beta v + F_{const}]}{-\beta} = \frac{1}{m} \cdot t + c$$

$$\ln[-\beta v + F_{const}] = \frac{-\beta}{m} \cdot t + c$$

$$-\beta v + F_{const} = c_2 Exp[\tfrac{-\beta}{m} \cdot t]$$

$$v = \frac{c_2 Exp[\tfrac{-\beta}{m} \cdot t] - F_{const}}{-\beta}$$

$$v(t) = c_3 Exp[\tfrac{-\beta}{m} \cdot t] + \frac{F_{const}}{\beta}$$

$$\text{where } c_3 = v(0) - \frac{F_{const}}{\beta}$$

$$v(t) = \left[v(0) - \frac{F_{const}}{\beta}\right] Exp[\tfrac{-\beta}{m} \cdot t] + \frac{F_{const}}{\beta}$$

REFERENCES

1. Astumian, R. D. Thermodynamics and Kinetics of a Brownian Motor. Science 276, 917-922 (1997).

2. Ajdari, A. Electrokinetic "ratchet" pump for Microfluidics (unpublished).

3. Ajdari, A. Pumping liquids using asymmetric electrode arrays. Physical Review E 61, R45-R48 (2000).

4. Bico, J. & Quere, D. Liquid trains in a tube. Europhysics Letters 51, 546-550 (2000).

5. Brown, A. B. D., Smith, C. G. & Rennie, A. R. Pumping of water with ac electric fields applied to asymmetric pairs of microelectrodes. Physical Review E 63 (2000).

6. Buguin, A., Talini, L. & Silberzan, P. Ratchet-like topological structures for the control of microdrops. Applied Physics A 75, 207-212 (2002).

7. Daniel, S. & Chaudhury, M. K. Rectified Motion of Liquid Drops on Gradient Surfaces Induced by Vibration. Langmuir 18, 3404-3407 (2002).

8. Gorre, L., Ioannidis, E. & Silberzan, P. Rectified motion of a mercury drop in an asymmetric structure. Europhysics Letters 33, 267-272 (1996).

9. Marquet, C., Buguin, A., Talini, L. & Silberzan, P. Rectified Motion of Colloids in Asymmetrically Structured Channels. Physical Review Letters 88 (2002).

10. Sandre, O., Gorre-Talini, L., Ajdari, A., Prost, J. & Silberzan, P. Moving droplets on asymmetrically structured surfaces. Physical Review E 60, 2964-2972 (1999).

11. Gallardo, B. S. et al. Electrochemical Principles for Active Control of Liquids on Submillimeter Scales. Science 283, 57-60 (1999).

12. Grunze, M. Driven Liquids. Science 283, 5398 (1999).

13. Daniel, S., Chaudhury, M. K. & Chen, J. C. Fast Drop Movements Resulting from the Phase Change on a Gradient Surface. Science 291, 633-636 (2001).

14. Barton, K. D. & Subramanian, R. S. The Migration of Liquid Drops in a Vertical Temperature Gradient. Journal of Colloid and Interface Science 133, 211-222 (1989).

15. Bico, J. & Quere, D. Self-propelling slugs. Journal of Fluid Mechanics 467, 101-127 (2002).

16. Brochard, F. Motions of Droplets on Solid Surfaces Induces by Chemical or Thermal Gradients. Langmuir 5, 432-438 (1989).

17. Brzoska, J. B., Brochard-Wyart, F. & Rondelez, F. Motions of Droplets on Hydrophobic Model Surfaces Induced by Thermal Gradients. Langmuir 9, 2220-2224 (1993).

18. Chaudhury, M. K. & Whitesides, G. M. How to Make Water Run Uphill. Science 256, 1539-1541 (1992).

19. Domingues Dos Santos, F. & Ondarcuhu, T. Free-Running Droplets. Physical Review Letters 75, 2972-2975 (1995).

20. Bain, C. D., Burnett-Hall, G. d. & Montgomerie, R. R. Rapid motion of liquid drops. Nature 372 (1994).

21. Ichimura, K., Oh, S.-K. & Nakagawa, M. Light-Driven Motion of Liquids on a Photoresponsive Surface. Science 288, 1624-1626 (2000).

22. Lee, S.-W. & Laibinis, P. E. Directed Movement of Liquids on Patterned Surfaces Using Noncovalent Molecular Adsorption. Journal of the American Chemical Society 122, 5395-5396 (2000).

23. Young, N. O., Goldstein, J. S. & Block, M. J. The motion of bubbles in a vertical temperature gradient. Journal of Fluid Mechanics 6, 350-356 (1959).

24. Scriven, L. E. & Sternling, C. V. The Marangoni Effects. Nature 187, 186-188 (1960).

25. Smoluchowski, M. Phys. Z. 13, 1069 (1908).

26. Feynman, R. P., Leighton, R. B. & Sands, M. The Feynman Lectures on Physics (Addison-Weseley, Redwood City, 1989).

27. Wasan, D. T., Nikolov, A. D. & Brenner, H. Droplets Speeding on Surfaces. Science 291, 605-606 (2001).

28. Adamson, A. W. Physical Chemistry of Surfaces (John Wiley & Sons, New York, 1976).

29. Levich, V. G. & Krylov, V. S. Surface-Tension-Driven Phenomena. Annual Review of Fluid Mechanics 1, 293-316 (1969).

30. Subramanian, R. S. in Transport Processes in Bubbles, Drops, and Particles (eds. Chhabra, R. P. & De Kee, D.) 1-42 (Hemisphere, New York, 1992).

31. Verlarde, M. G., Rednikov, A. Y. & Ryazantsev, Y. S. Drop motions and interfacial instability. J. Phys.: Condes. Matter 8, 9233-9247 (1996).

32. Chandra, S. & Aziz, S. D. Leidenfrost Evaporation of Liquid Nitrogen Droplets. Journal of Heat Transfer 116, 999-1006 (1994).

33. Whalley, P. B. Boiling, Condensation, and Gas-Liquid Flow (eds. Acrivos, A., et al.) (Clarendon Press, Oxford, 1987).

34. Hsu, Y.-Y. & Graham, R. W. Transport Processes in Boiling and Two-Phase Systems (eds. Hartnett, J. P. & Irvine, T. F., Jr.) (McGraw-Hill, Washington, 1976).

35. Gottfried, B. S. & Bell, K. J. Film Boiling of Spheroidal Droplets. I&EC Fundamentals 5, 561-568 (1966).

36. Gottfried, B. S., Lee, C. J. & Bell, K. J. The Leidenfrost Phenomenon: Film Boiling of Liquid Droplets on a Flat Plate. International Journal of Heat Mass Transfer 9, 1167-1187 (1966).